Journal of Rare Earths 39 (2021) 340–347

Contents lists available at ScienceDirect

Journal of Rare Earths

journal homepage: http://www.journals.elsevier.com/journal-of-rare-earths

Preparation of Al-based amorphous coatings and their properties☆

Lei Jin [a, b, c, *], Le Zhang [a], Kaige Liu [b], Zhigang Che [a], Kai Li [b], Ming Zhang [b], Bo Zhang [b]

[a] Science and Technology on Power Beam Process Laboratory, AVIC Manufacturing Technology Institute, Beijing 100024, China
[b] Department of Materials Application Research, AVIC Manufacturing Technology Institute, Beijing 100024, China
[c] Aeronautical Key Laboratory of Advanced Surface Engineering Technology, AVIC Manufacturing Technology Institute, Beijing 100024, China

ARTICLE INFO

Article history:
Received 24 October 2019
Received in revised form
6 April 2020
Accepted 29 April 2020
Available online 8 May 2020

Keywords:
Al-based amorphous material
Coatings
Cold spray
Properties
Rare earths

ABSTRACT

$Al_{86}Ni_8Co_1La_1Y_2Gd_2$ amorphous coatings were prepared using cold gas kinetic spray technology. The results show that $Al_{86}Ni_8Co_1La_1Y_2Gd_2$ amorphous coatings are achieved with the porosity about 3.2%, thickness about 893 μm, the amount of amorphous phase about 82.5%, the hardness about $300HV_{0.2}$. The corrosion potential and anti-corrosion life of 7075 T6 alloy aluminum are about −0.78 V and 72 h, respectively. The electrochemical analysis and neutral salt spray are about −0.69 V corrosion potential and 274 h anti-corrosion life for amorphous Al-based coatings, respectively. Therefore, the life of the Al-based amorphous coatings is about 3.8 times that of 7075 T6 aluminum alloy. Besides, the failure mechanism was analyzed using TEM in this investigation. In a word, $Al_{86}Ni_8Co_1La_1Y_2Gd_2$ coatings keep dense structure, high amorphous content, favorable amorphous phase stabilizing ability and longer anti-corrosion life. That is, $Al_{86}Ni_8Co_1La_1Y_2Gd_2$ coatings have better comprehensive properties. Therefore, these findings indicate that the present $Al_{86}Ni_8Co_1La_1Y_2Gd_2$ amorphous coatings prepared using cold gas kinetic spray technique can protect aluminum alloy very well and they can be considered to be used in aviation field.

1. Introduction

It is known that amorphous materials show excellent corrosion resistance in marine climate environments or other corrosion condition.[1,2] Therefore, amorphous materials show great potential for corrosion protection of light alloys such as Mg alloys and Al alloys. Most of the present reports refer to C-based, Cu-based, W-based and Fe-based bulk materials or some kinds of the corresponding coatings.[3–7] For coatings, the preparation methods mainly refer to air plasma spray (APS), high velocity oxygen fuel (HVOF), CVD, pulsed laser deposition, and some other methods. The problems how the advantages are kept and disadvantages are avoided further for Cu-based, W-based and Fe-based materials in industry need to be solved. Among many methods, cold gas kinetic spray (CS) has been proved to be an effective technique in the present. It can deposit coatings through solid-state plastic deformation of particles generating high strain rate (10^7–10^9 s^{-1}) under impact, which can remain the amorphous structure very well.[8,9] In the mean time, the low temperature characteristic of cold spray makes it suitable to deposit heat-susceptible materials (for example, amorphous, low-melting-point metal, nanostructure materials and organics) on various substrates. Therefore, combing amorphous materials and CS technology becomes a wonderful approach to fabricating Al-based amorphous coatings.[10]

Al-based metallic glasses (amorphous) exhibit high strength (above 1000 MPa, 3–4 times higher than crystalline counter parts), low density (3.2–3.7 g/cm^3), excellent corrosion and wear properties in reports.[11,12] For example, Lahiri et al. prepared amorphous powder and sprayed them on aluminum alloy.[13] Their results indicate that the ability of corrosion and friction of amorphous coatings improved by 5 and 6 times, respectively. Zhang et al. also found that $Al_{85}Ni_5Y_{10}$ amorphous alloy had better anti-corrosion properties than those of pure Al and aluminum alloys in 0.25 mol/L NaOH and 1 mol/L HCl liquor.[14] But some scientists do not describe the detail designs, properties of Al-based amorphous powders and more features of the corresponding coatings. Still less kinds of Al-based amorphous coatings were described in previous studies[15–17] and some properties were not involved systemically.[18]

Therefore, cold spray technology was carried out to fabricate Al-based amorphous coatings using $Al_{86}Ni_8Co_1La_1Y_2Gd_2$ amorphous powder we self-developed and then key properties, such as micro-

☆ **Foundation item:** Project supported by the AVIC Unite Fund (KZ041605114) and Civil Aircraft (MJ-2016-F-16).
* Corresponding author.
E-mail address: yugongyishanjin@126.com (L. Jin).

https://doi.org/10.1016/j.jre.2020.04.018
1002-0721/

structure, hardness, adhesive strength, anti-corrosion ability, were discussed systemically in this study. The aim of this study was to enrich Al-based amorphous powder material, investigate the more properties and expand application scope of Al amorphous material, which can give more guild and reference for industry application, such as fighters even the repair of composite materials.[19,20]

2. Experimental

2.1. Powder materials design and preparation

Firstly, $Al_{86}Ni_8Co_1La_5$ was adopted, and then both Y and Gd were added into $Al_{86}Ni_8Co_1La_5$ to replace La element. Y was added by 0 at%, 2 at%, 4 at%, respectively. The purity of all raw materials is higher than 99.9%. The master alloys were re-melted for four times for composition homogeneity under argon atmosphere. Then thin amorphous alloy film samples (ribbons) were manufactured using the single roller melt spinning method. The quenching rate was adjusted by the linear velocity of the copper roller which were 5 and 3 m/s, respectively. After the optimized chemical compositions were achieved, the same alloy was atomized under Ar gas to get amorphous powder. Its melt temperature and gas pressure were 1100 °C and 1.2 MPa in the gas pulverization, respectively. In the end, $Al_{86}Ni_8Co_1La_1Y_2Gd_2$ chemical composites were confirmed and the $Al_{86}Ni_8Co_1La_1Y_2Gd_2$ amorphous powder with sizes smaller than 15 μm was used to spray in this investigation.

Besides, 7075 T6 aluminum alloys were chosen as substrate material, and some properties of Al-based amorphous coatings were compared as 7075 T6 aluminum alloys.

2.2. Coatings prepared using cold spray

The aimed amorphous materials coatings were prepared using the DWCS-2000 cold spraying system (Shanxi DW Automation Co., Ltd., China) with a maximum operating pressure of 4 MPa, temperature of 800 °C and operated with nitrogen gas. Spraying distance (30 mm), gun traverse speed (300 mm/s) and powder velocity (20 g/s), powder size (4–15 μm) were fixed and the gas temperature was also confirmed (300 °C), which is marked as CS Al-based amorphous coatings.

2.3. Micro-structure measurements and phase compositions

The phase composition of the powder and coatings were characterized by X-ray diffraction (XRD) using a Philips XRD diffractometer with Cu Kα radiation.

The morphology of the powder and coatings were characterized by scanning electron microscopy (SEM, ZEISS super-55) and the porosity of coatings was measured based on image analysis with the Image J software (using gray scale analysis method).

An X-ray energy dispersive spectrometer (EDS) and transmission electron microscopy (TEM, JEM-ARM200F) were also used to examine some message, for example, the element distributions, micro-structure and phase compositions of the coatings.

2.4. Thermal behavior measurements

The thermal behavior of the coatings was investigated by a differential scanning calorimeter (DSC204F1 produced by NETZSCH of Germany) with different heating rates (10, 15, 20 and 30 °C/min) in a flowing argon atmosphere.

2.5. Hardness testing and adhesion strength

Hardness of coatings was measured using a Vicker hardness sclerometer. Force of 0.2 kg was loaded onto the cross section of coatings/substrate system and then the force was kept until 15 s, i.e., every 50 μm from the top side of the coating to the inner of substrate. The hardness was logged as $HV_{0.2}$.

The adhesive strength of each sample was measured at room temperature according to HB 5476-1991 standard. In this method, E−7 hot setting adhesive was applied and coatings were bonded to a metal stainless steel cylinder. These specimens for the adhesive strength test were put in the oven at 100 °C for 3 h. The tensile strength was obtained from the ratio of the maximum load applied at rupture by the cross-section area. To obtain more reliable values, 5 samples were tested and the average value was taken.

2.6. Anti-corrosion test

Electrochemical behavior of metal substrate and amorphous coatings was examined by a PARSTAT4000 electrochemical workstation. All measurements were carried out in a 1.5 L standard three-electrode glass cell. A platinum plate was used as the counter electrode while a saturated calomel electrode (SCE) was the reference electrode. The tests were carried out in 3.5 wt% NaCl solution at room temperature and pH value was about 7.0. The electrochemical samples were polished along with the curved surface before being sealed in epoxy resin just leaving the surface of coatings exposed to solutions. Prior to the tests, the air formed passive film of the working electrodes was cathodically removed by polarizing to −1.2 V vs SCE for 180 s. Afterward the samples were left at open circuit potential for about 1 h until the potential had reached a steady state. Ac impedance spectrum was done under the same condition.

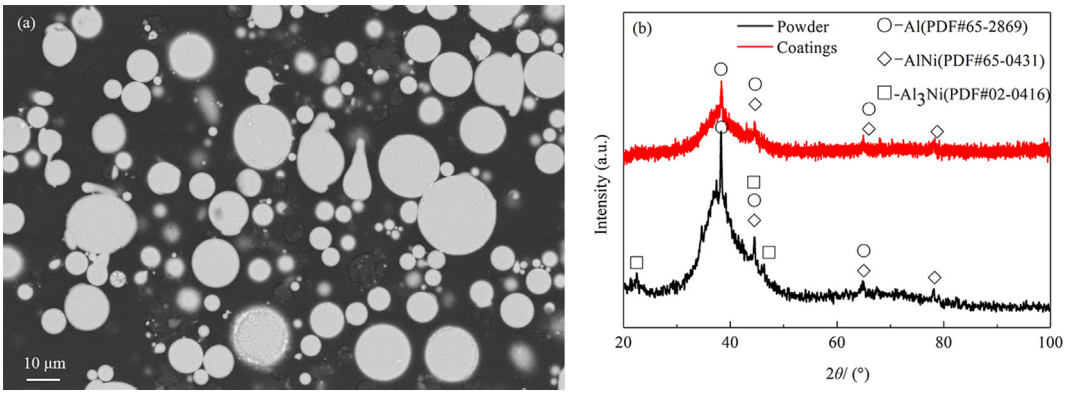

Fig. 1. Morphology (a) and XRD pattern (b) of Al-based amorphous powders and coatings.

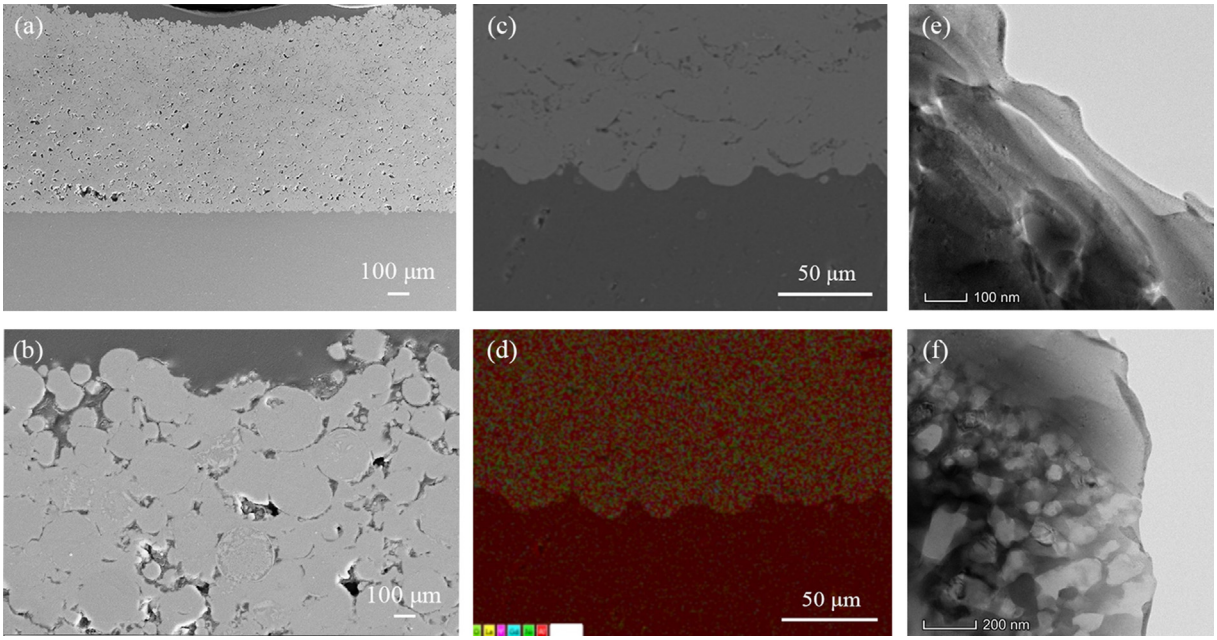

Fig. 2. Cross sections of amorphous coatings (a, b), the corresponding EDS images (c, d) and the TEM images of coatings (e, f).

Neutral salt fog corrosion performance was tested according to the GB10127-2002, the concentration of salt fog was 5.0 wt%, and the temperature was about 35 °C. The more details can be found in the literature.[21,22]

3. Results and discussion

3.1. Micro-structure analysis

The size of $Al_{86}Ni_8Co_1La_1Y_2Gd_2$ amorphous powder particle is between 4 and 15 μm (shown in Fig. 1(a)). Due to smooth surface and good flowing of powder, they will be directly used for cold spray. The XRD (Fig. 1(b)) measurements showed that Al amorphous particles had an amorphous content of about 92.4 wt% using Pseudo-Voigt methods.[23] Nearly all of the powder shows amorphous structure. The other crystal phases are mainly Al, AlNi and Al_3Ni phases using Jade 5.0 analysis software. Crystal phases existing were mainly attributed to lower cooling velocity using gas atomization process, but the results are satisfactory.

In Fig. 2(a,b), they easily show that the coatings have dense cross-sections, and less internal pores and micro-cracks. It can be calculated that the porosity is just about 3.2% analyzed using Image J software. This can be attributed to the enhanced plastic deformation of the particles during impact. Higher gas temperature and

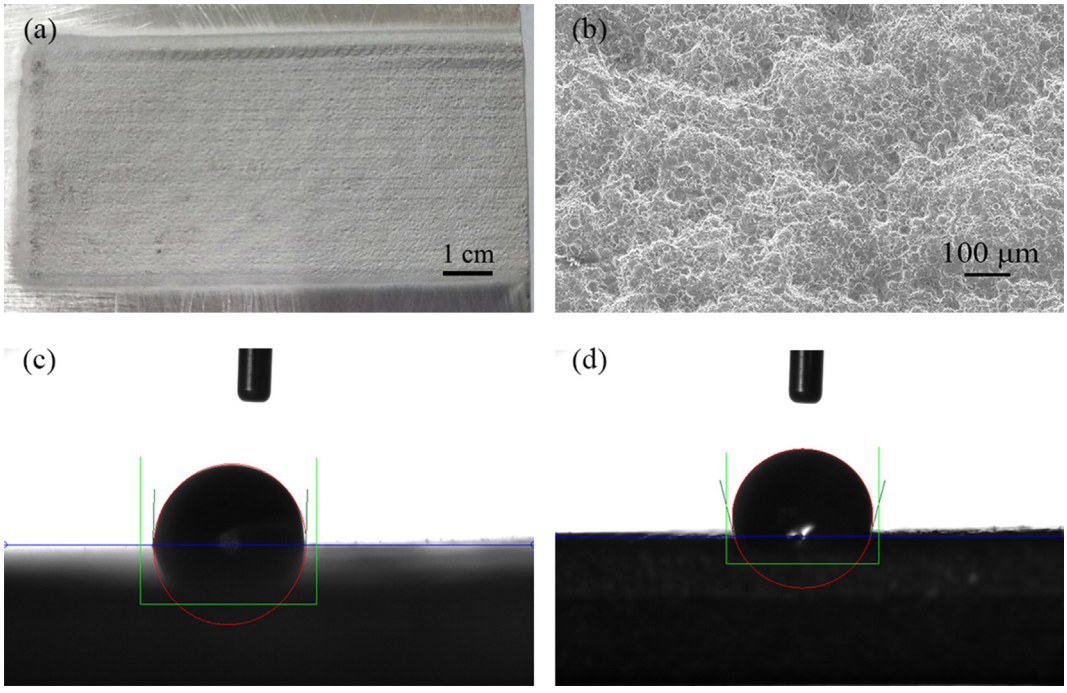

Fig. 3. Surface morphologies of CS amorphous coatings (a, b) and the contact angle (c, d).

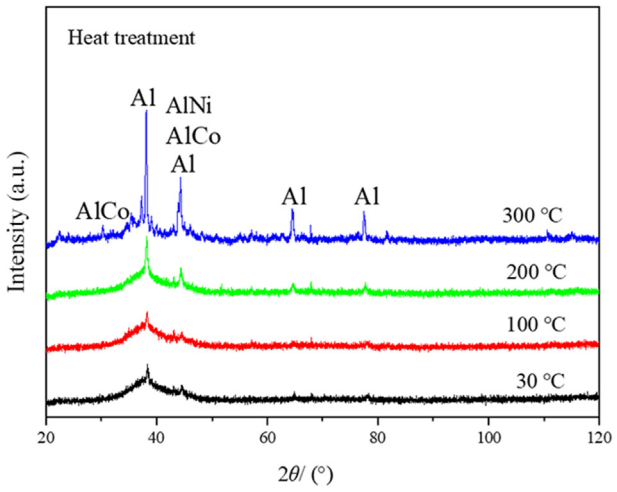

Fig. 4. XRD characteristics of the Al based amorphous coatings under different heat treatment temperatures.

gas pressure lead to higher particle velocity and following enhanced softening. The thickness of coatings was more than 893 μm, which indicated that these $Al_{86}Ni_8Co_1La_1Y_2Gd_2$ amorphous powders had the suited plastic deform ability and toughness in the present designs. This study illuminated also that the original higher hardness for amorphous powder was avoided, and some design difficulties were solved. So our composites and the corresponding CS technique parameters were acceptable and relatively ideal. And then the cross section was magnified and then it easily showed that some crystal phase appeared. It also signified that not all of the amorphous phase was preserved. Less high velocity flying particles produced some crystal phenomenon but most of them maintained primary structure unreservedly.

The EDS mapping results of the coatings are displayed in Fig. 2(c,d). According to the EDS analysis, the atomic proportion of the coatings was nearly equal to the nominal composition of the original amorphous powder and elements distribution was homogeneous. There were quite a few oxygen elements (0.62 wt%) found in the as-sprayed amorphous coatings, which were attributed to higher stabilization of powder and lower temperature cold spray. Consequently, the oxidation and thermal deterioration of the as-sprayed materials are significantly reduced, and this result generates extremely low oxide content for high-impact coatings. The service life of the coating can be prolonged and the service ability can be enhanced for the formation of the amorphous/nano crystalline phases.[24]

3.2. Wettability analysis of the amorphous coatings

In Fig. 3(a), it can be easily found that the coatings exhibited more uniform surface morphology although it was not very smooth. The main reason is the technical parameter-interval of spray gun. So the next aim is to control the suitable interval of spray gun and then the very smooth surface can be obtained. In order to investigate the characters of surface, the surface was magnified in Fig. 3(b), and it indicated that some little pores exist on the surface. What is the effect of these little pores, deteriorate or improve the properties? This question will be answered and discussed as follows.

The wettability of the coatings was characterized by contact angles (as shown in Fig. 3(c,d)). Results show that the coatings obtain high contact angles to neutral salt waters, and it possessed amphiphobicity. As can be seen from the round-likely roundness (as shown in Fig. 3(b)), the highly rough surface is mainly composed of small particles. At the same time, a large amount of air was stored between small holes due to its micro-structure, enabling the salt water droplets to stand on the coatings and nearly keep sphere shape. As a result, the droplets will not expand and they could easily slide from the surface. To our surprise, most of APS and HVOF have the opposite characteristic compared with the CS coatings; although some scientists also proved that Fe-based amorphous coatings by HVOF still possess robust hydrophobic.[24–27] However, what we found means that CS is also suitable to prepare amphiphobicity function coatings. The main reason is the low temperature cold spray technology, which does not melt and spread the flying particle. So the coarse surface was obtained and it is beneficial to obtaining amphiphobicity structure.

3.3. Analysis of compositions stability

In order to investigate further the phase stability of amorphous coatings, amorphous coatings were chosen to be thermal treated for 0.5 h under 4 different temperatures (30, 100, 200, 300 °C), and the XRD phase identification results are shown in Fig. 4, which suggests that there is a broad halo peak at $2\theta = 30°–50°$, along with a negligible amount of crystal structure present in the as-sprayed CS coatings. Crystalline phases present in the coatings were identified as Al, AlCo and AlNi phases, and exhibited a slight tendency towards a crystalline with the increase of heat treatment temperature (30, 100, 200, 300 °C). Furthermore, proportion of amorphous phase (300 °C heat treatment) decreased sharply compared with the 30, 100 and 200 °C heat treatment, and the value was about 82.5%. Under this condition, the coatings were mainly composed of Al phases, AlCo and AlNi phases, a portion of amorphous structure disappeared. It indicated that CS amorphous coatings could endure

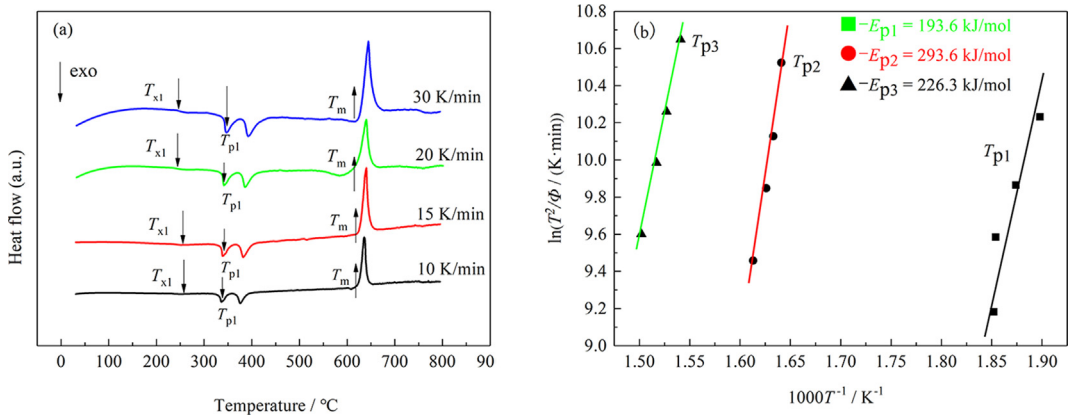

Fig. 5. DSC (a) and crystal growth activation energy (b) of the cold spray amorphous coatings.

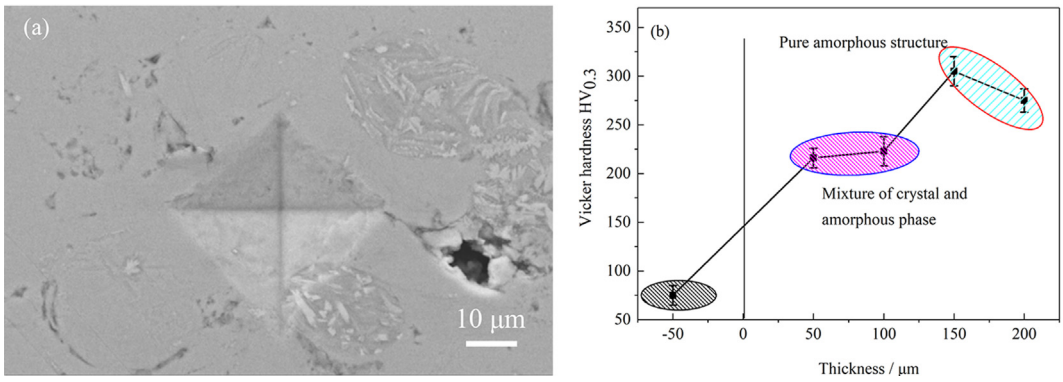

Fig. 6. The typical morphology of Vicker hardness (a) and statistics value for cross section of aluminum alloy and two different coatings zones (b).

200 °C for a long time. When the temperature was higher than 200 °C, CS coatings would produce more crystal phases. Therefore, this kind of amorphous coatings could be serviced at 200 °C high temperature not exceeding 300 °C.

Differential scanning calorimeter are good ways to understand stability of amorphous coatings and the relevant results are shown in Fig. 5. As observed in Fig. 5(a), the DSC traces of the coatings displayed an exothermic reaction above the crystallization temperature (T_x); this feature, associated with a decrease in heat flow, is thought to be associated with the production of certain crystalline phases. Particularly, the region of 319–398 °C (the larger exothermic peak) indicated that the amorphous coatings can keep stable just under 300 °C and the crystal temperature is about 350 °C. If the temperature is over 350 °C, these coatings will quickly crystallize and the key properties will deteriorate. This temperature is very important to judge the reaction of crystallization and high temperature stability in industry application.

Crystal growth activation energy of the coatings was an important instruction for physicochemical properties of material. Therefore, it is considered and calculated using the related equation from Kissinger model:[28]

$$\ln(T^2/\Phi) = -E/RT + C \quad (1)$$

where, Φ is the heating rate, T the characteristic temperature, E the crystallization activation energy, and R gas constant.

The related parameters were obtained and the results are shown in Fig. 5(b). E_{p1}, E_{p2} and E_{p3} were 193.6, 293.6 and 226.3 kJ/mol,

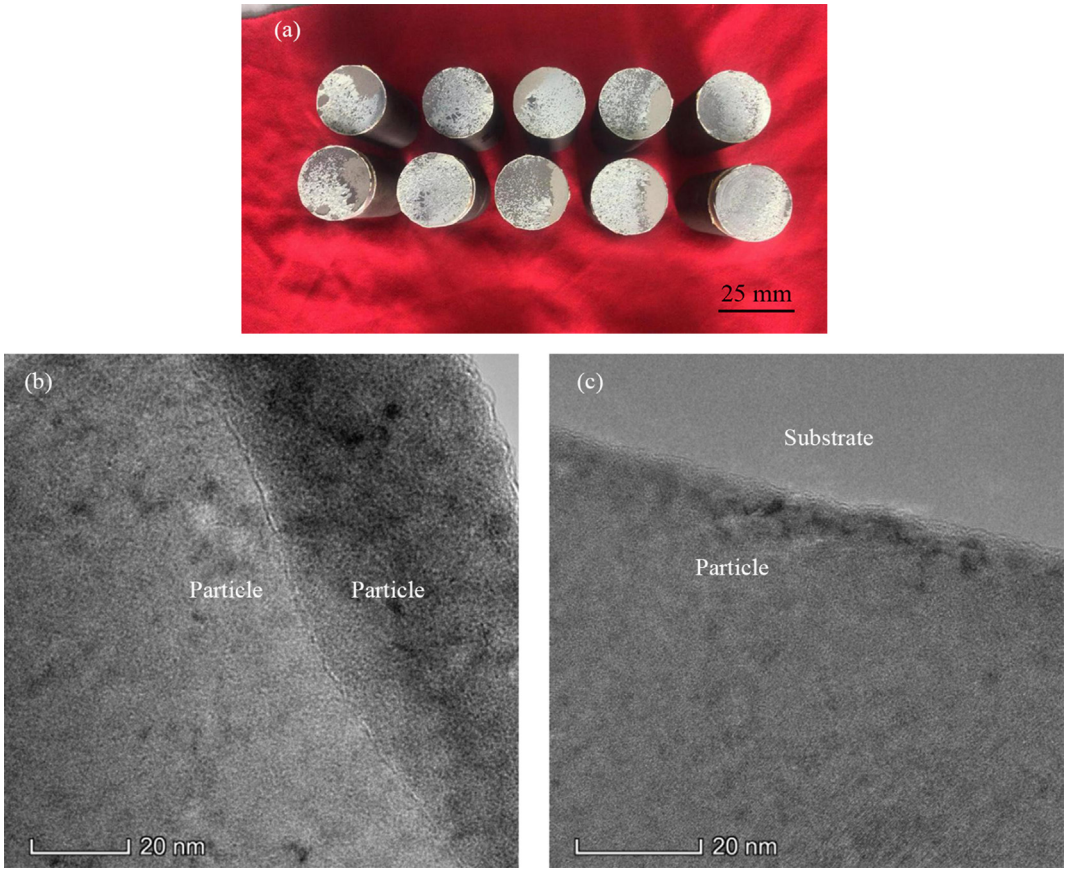

Fig. 7. Surface morphology of CS amorphous coatings after tensile test (a), the morphology of particle and particle (b), particle and substrate (c).

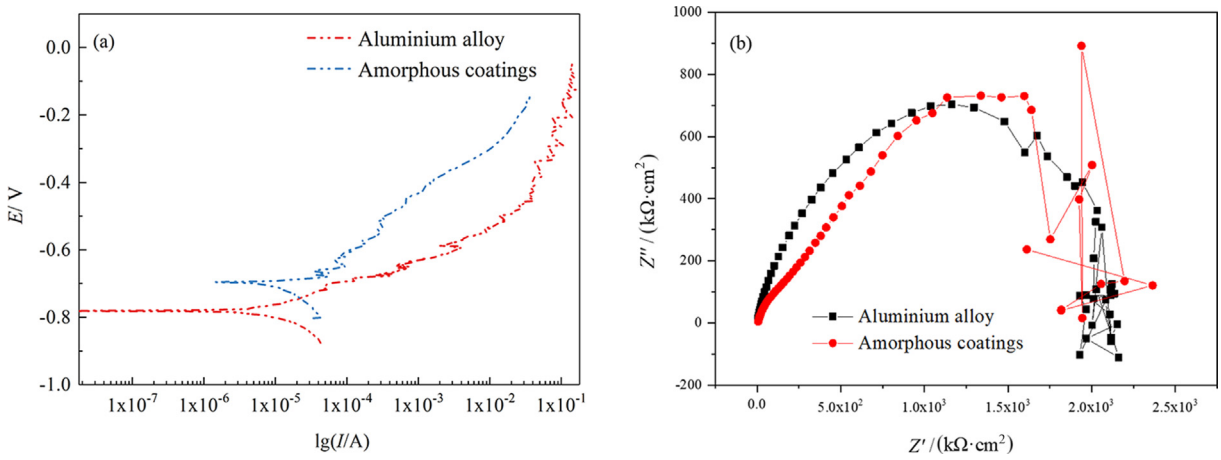

Fig. 8. Polarization (a) and Nyquist (b) curves for aluminum alloy and amorphous Al based amorphous coatings.

respectively. Generally speaking, crystal growth activation energy is higher and the crystal is more stable based on previous classics theory. According to previous report, Phan et al. find that their activation energy (E_{a1}) of Al based amorphous alloy is 313 kJ/mol. The α-Al phase crystallization activation energy (193.6 kJ/mol) of $Al_{86}Ni_8Co_1La_1Y_2Gd_2$ alloy is larger than that of $Al_{88}Ni_4Y_6Er_2$ (146.2 kJ/mol). The second peak (255.2 kJ/mol) is larger than that of $(Al_{80}Ca_8Li_6)_{97}La_3$ (the second peak is about 174.5 kJ/mol), demonstrating that $Al_{86}Ni_8Co_1La_1Y_2Gd_2$ amorphous coatings exhibit higher glass thermal stability although their raw material, preparation process and the related parameters were mostly different from ours.

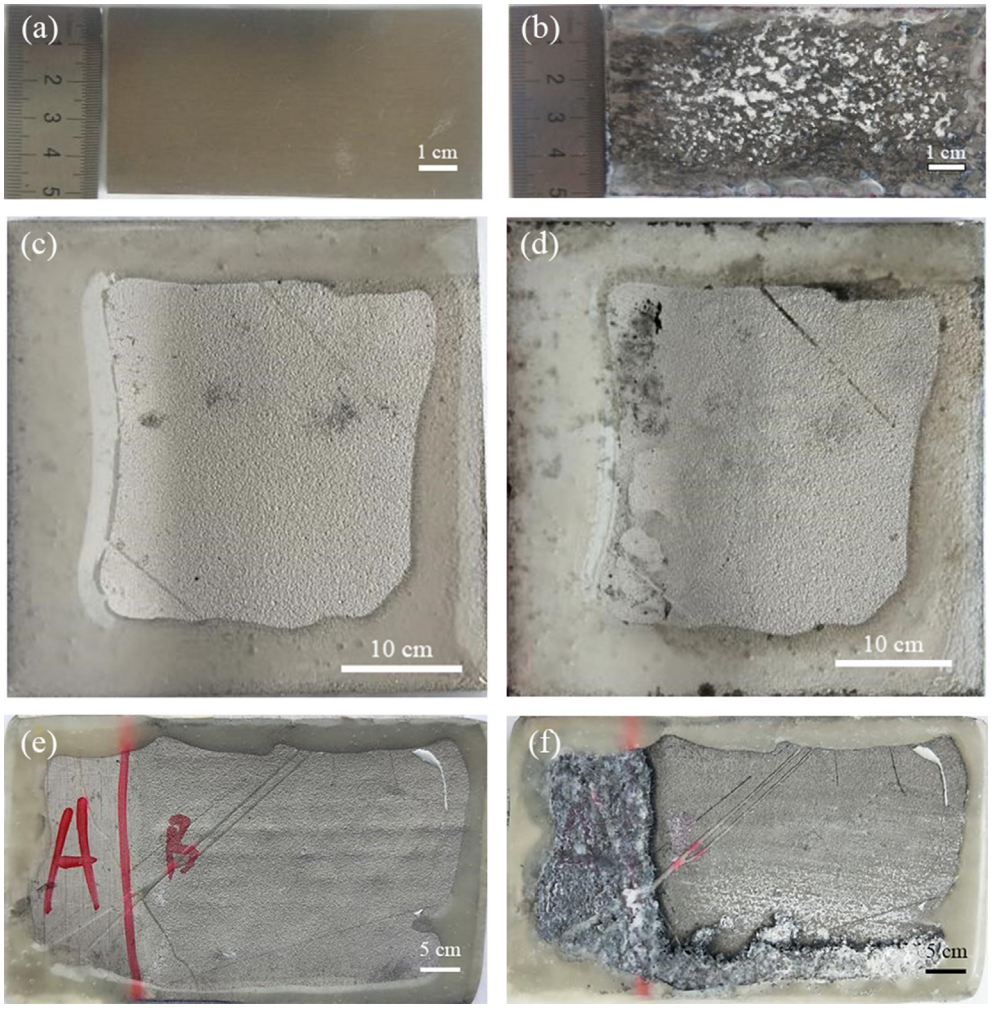

Fig. 9. Macro appearance of the aluminium alloy (a, b), amorphous coatings (c, d), mixture of alloy and coatings (e, f) under different time.

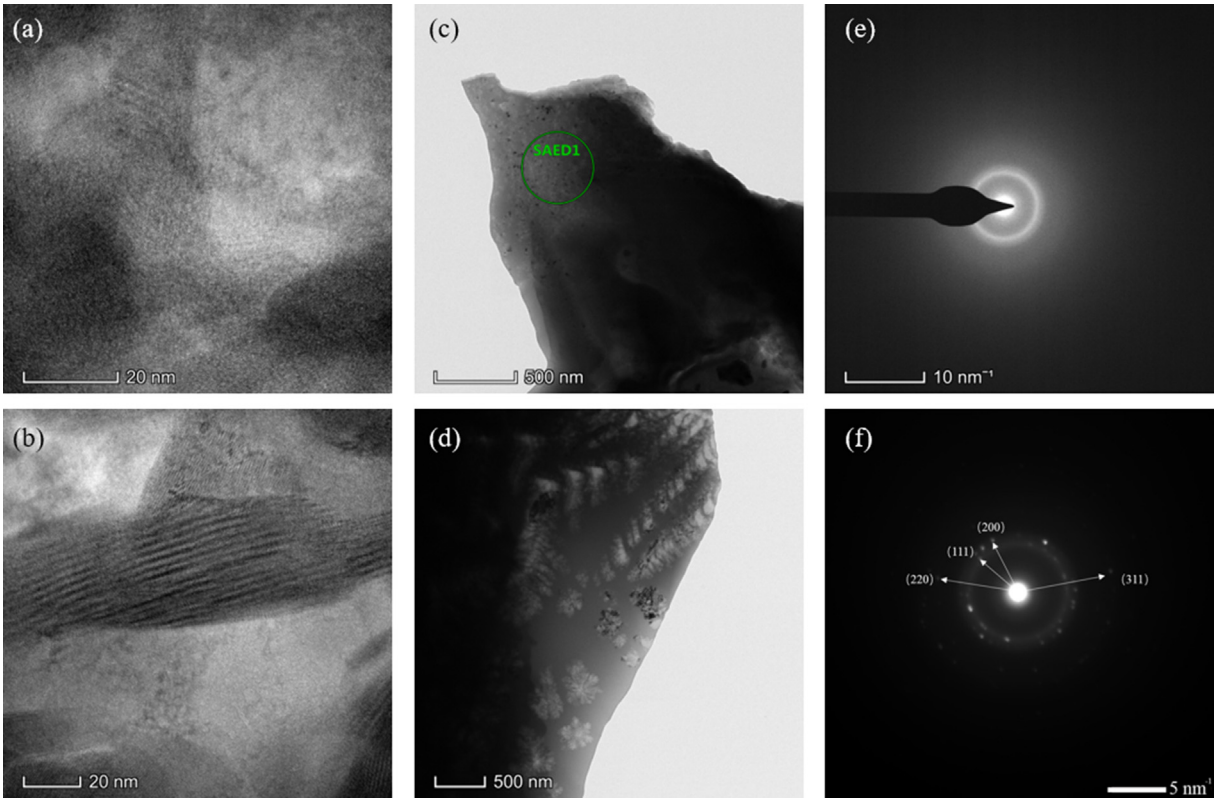

Fig. 10. Typical TEM images of CS amorphous figure before (a, c, e) and after (b, d, f) corrosion.

3.4. Hardness and adhesive strength

Hardness of coatings was measured using the Vicker hardness sclerometer and the results are demonstrated in Fig. 6. It indicated that the maximum hardness of the coatings was up to ~305 $HV_{0.2}$, which was significantly higher than that of the 7075 aluminum substrate (the value was just about 75 $HV_{0.2}$). The main reason comes from hard amorphous phase, which has higher hardness than aluminum alloy or Al crystal. In testing process, some phenomena were also found that hardness was increased with the increase of the amorphous concentration. When structures were mixed with amorphous and less crystal phase, the mean hardness was decreased. Moreover, it should be mentioned that the preserve of amorphous plays an important role in increasing the micro-hardness of such as coatings. In other words, amorphous phase should show excellent wear resistance under the dry sliding condition.

The measured average value of adhesion strengths between amorphous coatings and aluminum alloy was about 65.2 MPa. According to previous scientists' research, most of the measured values were in the range of 60–70 MPa for cold spray coatings, although the powder materials and technical parameters of us were basically different from the previous reports.[25,26] Ultimately, the measured adhesion strengths were eligible and satisfying in this research, and our results can give some references for the future research.

The surface micro-graph of rupture specimen after tensile testing is displayed in Fig. 7(a). It shows that the fracture occurred on the interface of binder/coat rather than on the interface of coat/metal substrate or in the inner of coatings. Therefore, it can also be judged that the real binding force between coatings and substrate is larger than that of 65.2 MPa. The deep reasons are not difficult to understand and some reasons are discussed as follows. CS contains excessive kinetic energy particles and then creates a very high temperature in a very short time (about 20–50 ns). Therefore, it is easy to form metallurgical bonding with metal substrate when the particles violently impact substrate (as shown in Fig. 7(b, c)). Besides, the high velocity will also form very dense structures and there is no space between particle and particle. As a result, CS has stronger adhesive strength than that of air plasma spray and arc spray (mechanical combine, loose micro-structure and some oxide inclusion). In a word, the higher kinetic energy and less oxidation for CS technique has the higher adhesive strength in this investigation.

3.5. Corrosion resistance

In this investigation, Al-based amorphous coatings were formed easily using cold spray. The key property of anti-corrosion was also explored and the methods were adopted using electrochemistry and neutral salt spray test methods.

The electrochemical results (Fig. 8(a)) were analyzed and the corresponding polarization voltage was −0.78 and −0.69 V for aluminum alloy and CS coatings, respectively. Ac impedance of them (Fig. 8(b)) can be detected that aluminum alloy had the minimum radius and CS coatings had the maximum radius. From two figures, the condensed conclusions can be given that CS coatings have better anti corrosion ability than that of aluminum alloy.

Macro appearance of pure aluminum alloy (Fig. 9(a, b)), pure amorphous Al based coatings (Fig. 9(c, d)), mixture of alloy and coatings (Fig. 9(e, f)) are displayed in Fig. 9 when they endure different neutral salt spraycorrosion time, respectively. The life of 7075 aluminum alloy and CS Al-based amorphous coatings was about 72 and 274 h, respectively. Comparing aluminum alloy and Al-based amorphous coatings, Al-based amorphous coatings had better properties than that of aluminum alloy although Al-based amorphous coatings were prepared under sub-optimal level of

technical parameters. That is, the mixture of the crystal and amorphous still had the excellent anti-corrosion properties. The better anti-corrosion properties are mainly from plentiful amorphous/nano crystalline phase, which are recognized to have an excellent wear-resistance, erosion-resistance and corrosion, which has been proved in previous investigations. Certainly, the key cause of good properties is derived from the dense micro-structure.

However, this kind of amorphous coatings suffered corrosion damage after 274 h neutral salt spray. Failure mechanisms need be discussed, as follows.

3.6. Failure mechanism

To reveal more details during corrosion and its breakdown, the micro structure and phase (TEM) were adopted and some results are presented in Fig. 10(a). Fig. 10(a–f) clearly present that large amounts of amorphous structure in the as-sprayed coatings became less and less with the extension of time. That is, the corrosion sample possessed some mixtures with plenty of amorphous structures and a small number of crystal structure under corrosion condition. Fig. 10(a, b) present that the particles were amorphous phase and interlock tightly each other, which is the main reason of higher adhesive strength, dense micro-structure, better anti-corrosion properties and other excellent properties. Besides, part of particles with nanostructure will also cause enhancement of materials' properties. Such as phenomenon and results have been reported and identified in previous investigation. For example, cold sprayed Al amorphous/nanocrystalline alloy coatings exhibit higher coefficient of friction (COF) and wear volume loss 68% greater than heat treated coatings.[19] However, the sample presents obvious crystal structure, which are dendrite morphology and alternate permutation (as shown in Fig. 10(d)).

The selected area diffraction (SAD) pattern exhibits the diffuse halo feature consisting of the diffuse diffraction spots and faint ring. Fig. 10(f) also shows that the crystal structure corresponds to (200) (311) (111) and (220), respectively. The spot pattern of SAD pattern reveals that the structure of α-Al is face-centered cubic structure (fcc), which is consistent with XRD pattern (Fig. 1(b)). Therefore, some regularity was given that these amorphous phases began to change into crystals, and crystal structures would produce growth stress, easily corrode and fail in the end. As a result, these crystal structures were destroyed after 274 h using 5 wt% NaCl neutral salt spray. So this corrosion process can be speculated that corrosion was accompanied by the phase transform of primitive amorphous structure.

4. Conclusions

The results show that $Al_{86}Ni_8Co_1La_1Y_2Gd_2$ can be sprayed easily by cold spray. The prepared amorphous coatings are dense and the porosity is just about 3.2%, and coatings can achieve a thickness of 893 μm. The glass/amorphous content is higher and the value is about 82.5% even at a high spraying temperature of 300 °C. The adhesive strength is about 65.2 MPa and the hardness is about 305 $HV_{0.2}$, which is much larger than that of 7075 aluminum alloy. The corrosion resistance under neutral salt spray is about 274 h and the life is about 3.8 times that of 7075T6 aluminum alloy. The CS Al amorphous coatings can protect the aluminum alloy very well under corrosion condition and the prepared coatings have better comprehensive properties. According to our results, the CS Al amorphous coatings should have a broad prospect in aviation and navigation industry.

References

1. Zhao X, Fang P, Tang YB, Chen YG, Zhou LT, Guo HQ. Corrosion behavior and magnetocaloric effect of FeNi (1J85) coated $LaFe_{11.6}Si_{1.4}$/Sn composites. *J Rare Earths*. 2019;37(6):633.
2. Wang Y, Jiang SL, Zheng YG, Ke W, Sun WH, Chang XC, et al. Effect of processing parameters on the microstructures and corrosion behavior of high-velocity oxy-fuel (HVOF) sprayed Fe-based amorphous metallic coatings. *Mater Corros*. 2013;64(9):801.
3. Jang YJ, Kang YJ, Kitazume K, Umehara N, Kim J. Mechanical and electrical properties of micron-thick nitrogen-doped tetrahedral amorphous carbon coatings. *Diam Relat Mater*. 2016;69:121.
4. El-Eskandrany MS, Al-Azmi A. Potential applications of cold sprayed $Cu_{50}Ti_{20}Ni_{30}$ metallic glassy alloy powders for antibacterial protective coating in medical and food sectors. *J Mech Behav Biomed Mater*. 2016;56:183.
5. Besozzi E, Dellasega D, Pezzoli A, Conti C, Passoni M, Beghi MG. Amorphous, ultra-nano- and nano-crystalline tungsten-based coatings grown by Pulsed Laser Deposition: mechanical characterization by Surface Brillouin Spectroscopy. *Mater Des*. 2016;106:14.
6. Wang G, Xiao P, Huang ZJ, He RJ. Microstructure and wear properties of Fe-based amorphous coatings deposited by high-velocity oxygen fuel spraying. *J Iron Steel Res Int*. 2016;23(7):699.
7. Vignesh S, Shanmugam K, Balasubramanian V, Sridhar K. Identifying the optimal HVOF spray parameters to attain minimum porosity and maximum hardness in iron based amorphous metallic coatings. *Defence Technol*. 2017;2(13):101 (in Chin).
8. Vilardell AM, Cinca N, Cano IG, Concustel A, Dosta S, Guilemany JM, et al. Dense nanostructured calcium phosphate coating on titanium by cold spray. *J Eur Ceram Soc*. 2017;37(4):1747.
9. Ko KH, Choi JO, Lee H, Seo YK, Jung SP, Yu SS. Cold spray induced amorphization at the interface between Fe coatings and Al substrate. *Mater Lett*. 2015;149:40.
10. Concustell A, Henao J, Dosta S, Cinca N, Canol G, Guilemany JM. On the formation of metallic glass coatings by means of Cold Gas Spray technology. *J Alloys Compd*. 2015;651:764.
11. Bassim N, Kiminami CS, Kaufman MJ. Phases formed during crystallization of amorphous $Al_{84}Y_9Ni_5Co_2$ alloy. *J Non-Cryst Solids*. 2000;273(1–3):271.
12. Inoue A, Sobu S, Louzguine DV, Kimura H. Ultrahigh strength Al-based amorphous alloys containing Sc. *J Mater Res*. 2004;19(5):1539.
13. Lahiri D, Gill PK, Scudino S, Zhang C, Singh V, Karthikeyan J, et al. Cold sprayed aluminum based glassy coating: synthesis, wear and corrosion properties. *Surf Coating Technol*. 2013;232(12):33.
14. Zhang HW, Wang JQ, Hu ZQ. Research and development of aluminum-based amorphous alloys. *Mater Rev*. 2001;15:7 (in Chin).
15. Tan CL, Zhu HM, Kuang TC, Shi Jeffery, Liu HW, Liu ZW. Laser cladding Al-based amorphous-nanocrystalline composite coatings on AZ80 magnesium alloy under water cooling condition. *J Alloys Compd*. 2017;690:108.
16. Gao SZ, Wei J, Jia JR, Liu L, Zhang T, Wang XM, et al. Fabrication and property of Al-Ce-Fe amorphous coating. *J Inner Mongolia Univ Sci Technol*. 2016;35(2):166 (in Chin).
17. Lawal J, Kiryukhantsev-Korneev P, Matthews A, Leyland A. Mechanical properties and abrasive wear behavior of Al-based PVD amorphous/nanostructured coatings. *Surf Coating Technol*. 2017;310(Complete):59.
18. Babu PS, Jha R, Guzman M, Sundararajan G, Agarwal A. Indentation creep behavior of cold sprayed aluminum amorphous/nano-crystalline coatings. *Mater Sci Eng, A*. 2016;658:415.
19. Ding M. Research on maintenance technology of composite rudder structure. *Sci Bull*. 2019;22:296 (in Chin).
20. Ding M. Research on anti-corrosion design of vertical tail fin of a certain type plane. *Sci Inf Tech*. 2019;625:131 (in Chin).
21. He JJ, Li J, Zhang SG. Influence of pre-electroplating Ni on resistance of Sn-8Zn coating to neutral salt spray corrosion. *Hot Work Technol*. 2013;42(24):177 (in Chin).
22. Wang S, Min JY, Lin JP, Wu YR. Effect of neutral salt spray (NSS) exposure on the lap-shear strength of adhesive-bonded 5052 aluminum alloy (AA5052) joints. *J Adhes Sci Technol*. 2019;33(5):549.
23. Sánchez-Bajo F, Cumbrera FL. The use of the Pseudo-Voigt function in the variance method of X-ray line-broadening analysis. *J Appl Crystallogr*. 1997;30(5–1):550.
24. Wang JX. *Study on micro-structure and properties of laser surface remelted Fe-based amorphous coatings*. Xi'an: Changan University; 2015 (in Chin).
25. Liu M, Yang K, Deng CM. Microstructure and properties of Cu coating fabricated onto diamond-Cu substrate by low-temperature HVOF process. *J Therm Spray Technol*. 2016;25(8):1.
26. Zhang C, Wu Y, Liu L. Robust hydrophobic Fe-based amorphous coating by HVOF. *Appl Phys Lett*. 2012;101:121603.
27. Li DY, Chen XY, Hui XD, Wang JP, Jin PP, Li H. Effect of amorphicity of HVOF sprayed Fe-based coatings on their corrosion performances and contacting osteoblast behavior. *Surf Coating Technol*. 2017;310:207.
28. Ko KH, Choi JO, Lee H. The interfacial restructuring to amorphous: a new adhesion mechanism of cold-sprayed coatings. *Mater Lett*. 2016;175:1.